

The AGN/starburst content in high redshift ULIRGs

Y. Watabe,^{1*} G. Risaliti,^{1,2} M. Salvati,¹ E. Nardini,³ E. Sani,³ A. Marconi³

¹*INAF-Osservatorio Astrofisico di Arcetri, L.go E. Fermi 5, 50125 Firenze, Italy*

²*Harvard-Smithsonian Center for Astrophysics, 60 Garden St. Cambridge, MA 02138 USA*

³*Dipartimento di Astronomia e Scienza dello Spazio, Università di Firenze, L.go E. Fermi 2, 50125 Firenze, Italy*

ABSTRACT

We apply a simple model, tested on local ULIRGs, to disentangle the active galactic nucleus (AGN) and starburst contributions in submillimeter and 24 μm -selected ULIRGs observed with the *Spitzer*-IRS spectrometer. We quantitatively estimate the average AGN contribution to the stacked 6–8 μm rest-frame spectra of these sources in different luminosity and redshift ranges, and, under the assumption of similar infrared-to-bolometric ratios as in local ULIRGs, the relative AGN/starburst contributions to the total infrared luminosity. Though the starburst component is always dominant in submillimeter-selected ULIRGs, we find a significant increase of the AGN contribution at redshift $z > 2.3$ with respect to lower z objects. Finally, we quantitatively confirm that the mid-infrared emission of 24 μm -selected ULIRGs is dominated by the AGN component, but the starburst component contributes significantly to the bolometric luminosity.

Key words: galaxies: active – galaxies: high-redshift – galaxies: nuclei – galaxies: starburst

1 INTRODUCTION

Infrared number counts and the cosmic infrared background provide strong evidence that Ultraluminous Infrared Galaxies (ULIRGs; e.g., Soifer et al. 1984; Sanders & Mirabel 1996; Blain et al. 2002; Lonsdale et al. 2006), i.e. sources with a total infrared luminosity, $L_{8-1000\mu\text{m}}$, greater than $10^{12}L_{\odot}$, are a key component of the high redshift Universe (e.g., Dole et al. 2001; Lagache et al. 2005; Le Floc'h et al. 2005). ULIRGs at high redshift have been discovered using different selections, leading to distinct populations. In particular, observations performed with the Submillimeter Common User Bolometer Array (SCUBA; Holland et al. 1999) on the James Clerk Maxwell Telescope (JCMT; e.g., Smail et al. 1997) discovered a new population of submillimeter galaxies (SMGs), distributed at $z = 1 - 3$ (median redshift is 2.3) (e.g., Chapman et al. 2005), and with estimated total infrared luminosity in the ULIRG range. We refer to these galaxies as submm-ULIRGs.

Another population of high- z infrared luminous galaxies has been discovered through 24 μm selection. For example, Houck et al. (2005) and Brand et al. (2007) have surveyed the Boötes field of the NOAO Deep Wide-Field Survey (NDWFS; Jannuzi & Dey 1999) with the Multiband Imaging Photometer for *Spitzer* (MIPS; Rieke et al. 2004) at 24 μm . Also, Yan et al. (2005) have reported the initial results

from a *Spitzer* GO-1 program to obtain low-resolution, mid-infrared spectra in the *Spitzer* First Look Survey (FLS). These 24 μm -selected ULIRGs (hereafter, 24 μm -ULIRGs) have also redshifts in the range $z = 1 - 3$ (Houck et al. 2005; Yan et al. 2005; Brand et al. 2007).

The properties of these high- z galaxies suggest that they are likely associated with an early phase in the formation of massive galaxies, supermassive black holes, and active galactic nuclei (AGNs). Therefore, making clear the origin of their energy sources for different redshift ranges is very important to understand the star formation history and the AGN activity in the high- z Universe. In this context, a key point to be investigated is the relative AGN/starburst contribution to the bolometric luminosity of these galaxies. Here we present a quantitative estimate of the AGN content in submillimeter and 24 μm -ULIRGs, based on a deconvolution method recently developed by our group for local ULIRGs (Nardini et al. 2008, hereafter N08) by means of *Spitzer*-Infrared Spectrograph (IRS; Houck et al. 2004) 5 – 8 μm spectroscopy. Throughout this paper we use a standard cosmology with $H_0 = 73\text{kms}^{-1}\text{Mpc}^{-1}$, $\Omega_M = 0.3$ and $\Omega_{\Lambda} = 0.7$.

2 SAMPLE DATA AND DATA REDUCTION

Our sample consists of all the submm- and 24 μm -selected sources with known redshift, and with an available *Spitzer*-IRS observation. The submm sample was obtained by combining the SCUBA detected sources from

* E-mail: watabe@arcetri.astro.it

submm-ULIRGs position	redshift	L_{IR}	ref.	P. ID	24 μm -ULIRGs position	redshift	L_{IR}	ref.	P. ID
SMM J002634.10+170833.7	2.73	0.46	2	3241	SST24 J142538.22+351855.2	2.26	4.9	5	12
SMM J023951.87-013558.8	2.81	2.29	2	3241	SST24 J142626.49+344731.2	2.13	5.2	5	12
SMM J030227.73+000653.5	1.408	2.63	1	20081	J142644.33+333052.0	3.355	2.39	7	12
SMM J094253.42+465954.5	2.38	5.79	2	3241	SST24 J142645.71+351901.4	1.75	0.5	5	12
SMM J094303.69+470015.5	3.36	0.83	2	3241	SST24 J142653.23+330220.7	1.86	0.8	5	12
SMM J105155.47+572312.7	2.67	0.46	2	3241	SST24 J142804.12+332135.2	2.34	0.8	5	12
SMM J105207.49+571904.0	2.69	2.67	2	3241	SST24 J142924.83+353320.3	2.73	1.5	5	12
SMM J105238.19+571651.1	1.852	0.55	1	20081	SST24 J142958.33+322615.4	2.64	1.7	5	12
SMM J123555.13+620901.6	1.875	0.6 [†]	1	20456	SST24 J143001.91+334538.4	2.46	4.2	5	12
SMM J123600.16+621047.3	1.994	0.96 [†]	1	20456	J143028.52+343221.3	2.176	0.92	7	15
SMM J123616.11+621513.5	2.578	0.66 [†]	1	20456	SST24 J143251.82+333536.3	1.78	2.6	5	12
SMM J123618.33+621550.4	1.865	0.64 [†]	1	20456	J143312.7+342011.2	2.2	1.20	7	15
SMM J123621.27+621708.1	1.988	0.69 [†]	1	20456	SST24 J143358.00+332607.1	1.96	0.6	5	12
SMM J123634.51+621240.9	1.219	0.36 [†]	1	20456	J143424.24+334543.4	2.26	0.74	7	12
SMM J123707.21+621408.1	2.484	1.23 [†]	1	20081	SST24 J143447.70+330230.6	1.78	0.8	5	12
SMM J123711.37+621331.1	1.996	0.5 [†]	3	20456	SST24 J143504.12+354743.2	2.13	0.8	5	12
SMM J123711.98+621325.7	1.992	0.28 [†]	1	20081	SST24 J143520.75+340418.2	2.08	0.9	5	12
MM J154127.28+661617.0	2.79	0.9	2	3241	SST24 J143523.99+330706.8	2.59	1.4	5	12
SMM J163639.01+405635.9	1.495	0.61	1	20081	SST24 J143539.34+334159.1	2.62	3.5	5	12
SMM J163650.43+405734.5	2.378	3.10	1	20081	SST24 J143644.22+350627.4	1.95	1.7	5	12
SMM J163658.78+405728.1	1.21	0.09	2	3241	IRS 9 J171350.001+585656.83	1.83	1.70	6	3748
SMM J163706.60+405314.0	2.38	0.64	2	3241	IRS 11 J171439.570+585632.10	1.8	0.55	6	3748
ERO J164502.26+462626.5	1.443	>0.18	4	13	IRS 8 J171536.336+593614.76	2.6	1.89	6	3748
SMM J221733.91+001352.1	2.555	0.77	1	20081	IRS 2 J171538.182+592540.12	2.34	4.07	6	3748
SMM J221735.15+001537.2	3.098	1.45	1	20081	IRS 1 J171844.378+59200.53	2.1	3.03	6	3748
SMM J221735.84+001558.9	3.089	1.24	1	20081					
SMM J221737.39+001025.1	2.614	2.02	1	20081					
SMM J221804.42+002154.4	2.517	0.72	1	20081					

Table 1. Submm- and 24 μm -ULIRGs sample. Column 1: Object position. Col. 2, 3, and 4: Redshift and infrared luminosity, in units of $10^{13} L_{\odot}$ ([†] (Pope et al. 2008)) and references therein; [1] Chapman et al. (2005); [2] Valiante et al. (2007); [3] Swinbank et al. (2004); [4] Greve et al. (2005); [5] Houck et al. (2005); [6] Yan et al. (2005); [7] Brand et al. (2007). Col. 5: Programs of the *Spitzer*-IRS observations.

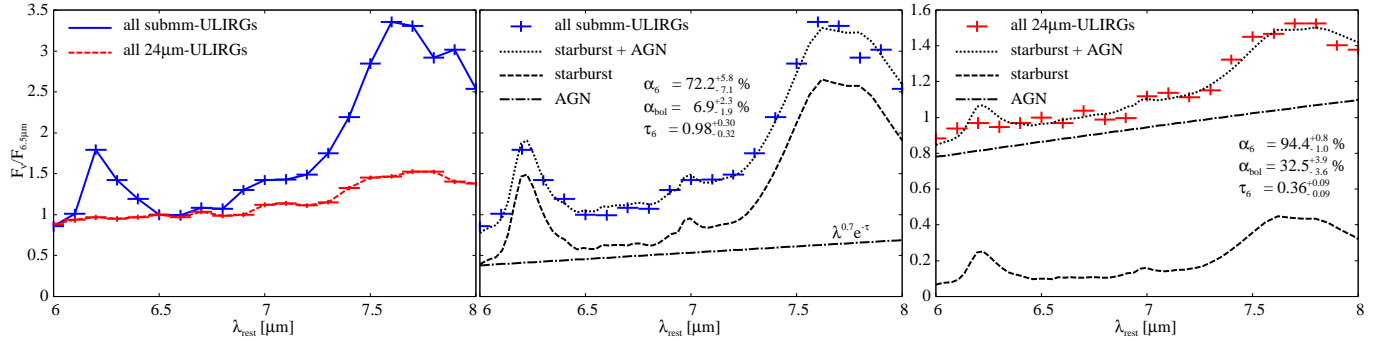


Figure 1. 6 – 8 μm rest-frame composite spectra of submm-ULIRGs and 24 μm -ULIRGs, with their best fit models. The flux density, F_{ν} are normalized at 6.5 μm . *Left:* Composite spectra for all submm-ULIRGs (solid blue line) and 24 μm -ULIRGs (dashed red line). *Middle and right:* Composite spectrum of the submm-ULIRGs and 24 μm -ULIRGs, respectively, with the best fit model (*dotted line*) and the AGN (*dashed dotted line*) and starburst (*dashed line*) components. α_6 and α_{bol} are the intrinsic AGN contribution to the 6 μm flux density (in percent) and the AGN contribution to the total infrared luminosity (in percent), respectively. τ_6 is the optical depth to the AGN at 6 μm .

Chapman et al. (2005) (submm bright, pre-selected in radio) and Valiante et al. (2007) (without radio pre-selection). These two subsamples are different in several respects (lensing properties, submm flux range, redshift distribution). However, their selection criteria are not expected to introduce any bias in their AGN content (we discuss possible effects in §4). The 24 μm sources are also selected in different ways through their 24 μm flux and different optical/infrared

colors (e.g. 24/8 μm , 24 $\mu\text{m}/R$). It is well known that these criteria are strongly biased toward sources whose mid-IR emission is dominated by the AGN component. Redshift, bolometric luminosities as well as other relevant data for all the sources are presented in Table 1. The bolometric luminosities listed in Table 1 are obtained by fitting a spectral energy distribution to the available data (see single references for details). The uncertainties on the single values

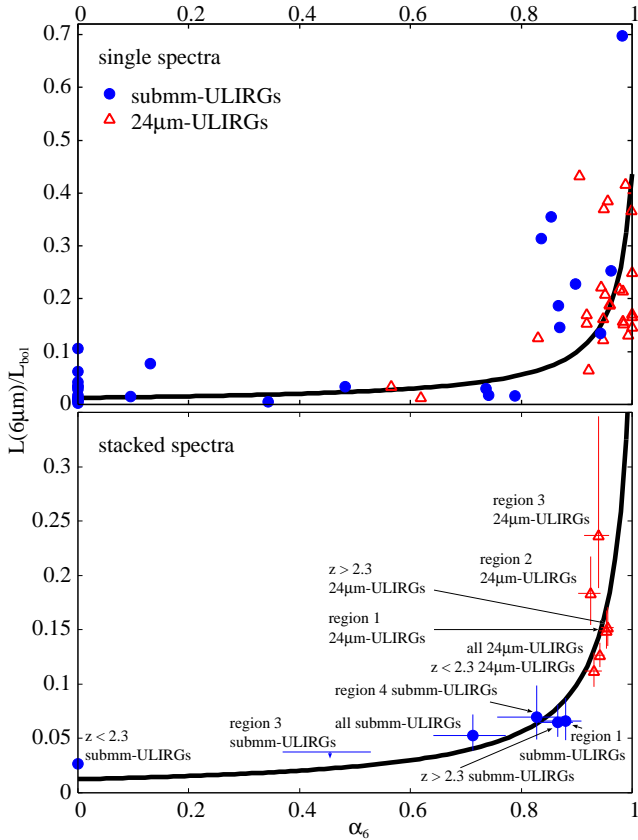


Figure 2. Upper panel: Absorption-corrected $6 \mu\text{m}$ /bolometric ratio versus the AGN fraction, α_6 , for submm-ULIRGs (*blue filled circle*) and $24 \mu\text{m}$ -ULIRGs sources (*red open triangle*). The continuous line refers to the best fit relation obtained for local ULIRGs (N08). Typical fit errors of x- and y- coordinates are a factor of 10% and 2 – 3, respectively. Lower panel: same for the stacked spectra of the subgroups discussed in the text.

can therefore be high (about 50% for submm sources, and a factor of three for $24 \mu\text{m}$ sources, since the mid-IR to bolometric correction is strongly dependent on the AGN/SB relative contribution). Data reduction has been performed with the SPICE 1.4.1 package, using the pipeline version S15.3, provided by the *Spitzer* Science Center. The coadded images have been background-subtracted by means of the two observations in the nodding cycle. The calibrated one-dimensional spectra for the positive and the negative beams were extracted using the “optimal” extraction mode in SPICE, and the two one-dimensional spectra averaged in order to obtain the final spectrum. Since we are interested in the average properties of the two populations, and the spectral quality is low, we stacked the spectra of the single sources, after shifting and re-sampling each spectrum to the rest-frame wavelengths and bin sizes. We also had a quick look at each single spectrum, in order to check that the stacked data are not dominated by individual objects with high S/N.

3 AGN AND STARBURST DECOMPOSITION MODEL

In order to separate the AGN and the starburst components for submm-ULIRGs and $24 \mu\text{m}$ -ULIRGs, we use the spectral decomposition model for local ULIRGs of N08. The model is based on the following main points: 1) in ULIRGs, the ratio between the $3 - 8 \mu\text{m}$ emission and the bolometric flux is 30 – 100 times higher for AGNs than for starbursts. The contrast rapidly decreases with increasing wavelength. 2) The starburst spectrum in this wavelength range shows little variation from source to source, and a template obtained by averaging the highest signal-to-noise pure starburst spectra fits well all the known starburst-dominated ULIRGs. 3) The AGN component can be represented with a power law $f_\nu^{\text{AGN}} \propto \lambda^{0.7}$ (Netzer et al. 2007), and an exponential attenuation $\exp(-\tau(\lambda))$, where the optical depth follows the conventional law $\tau(\lambda) \propto \lambda^{-1.75}$ (Draine 1989). In this assumption, the total flux density is written as follows,

$$f_\nu^{\text{obs}}(\lambda) = \eta_{\text{SB}} f_\nu^{\text{SB}} + \eta_{\text{AGN}} f_\nu^{\text{AGN}} e^{-\tau(\lambda)}, \quad (1)$$

where η_{SB} and η_{AGN} are the flux density amplitudes of the starburst and AGN templates f_ν^{SB} and f_ν^{AGN} normalized at $6 \mu\text{m}$, respectively. We can estimate the only two free parameters (the ratio of η_{SB} to η_{AGN} and τ_6 , which is the $6 \mu\text{m}$ optical depth to the AGN) by fitting the spectrum. From these, we can get the intrinsic AGN contribution to the $6 \mu\text{m}$ flux density, $\alpha_6 = \eta_{\text{AGN}} / (\eta_{\text{AGN}} + \eta_{\text{SB}})$. In addition, we can also estimate the AGN contribution to the total infrared luminosity (this roughly corresponds to the bolometric luminosity, L_{bol} , for ULIRGs), $\alpha_{\text{bol}} = \eta_{\text{AGN}} / (\eta_{\text{AGN}} + K \eta_{\text{SB}})$, where $K = R^{\text{AGN}} / R^{\text{SB}}$, and R^{AGN} and R^{SB} are the ratios of the intrinsic flux at $6 \mu\text{m}$ to the total infrared flux of AGN and starbursts, respectively; in local ULIRGs, $\log R^{\text{AGN}} = -0.36^{+0.06}_{-0.07}$, $\log R^{\text{SB}} = -1.91^{+0.02}_{-0.02}$, yielding $K \sim 35$ (Nardini et al. in prep.). The model has been successfully applied to a sample of local ULIRGs, obtaining two important results: 1) despite the complexity of the spectra, all the sources were successfully fitted, showing that the relative AGN/starburst contribution and the extinction of the AGN component are responsible for most of the observed variety; 2) the expected AGN/starburst contributions to the bolometric luminosity reproduce closely the total observed luminosity. This is an important test for our model: the bolometric contributions are obtained from the $6 \mu\text{m}$ spectral decomposition only (and from the average bolometric ratios, which have a fixed value for all objects), therefore the comparison between the predicted and observed total luminosities is an independent check of the results.

Here we apply the same model to high-redshift sources. In doing so, we assume that a) the intrinsic SED, and b) the bolometric ratios, are the same at low and high redshift. We discuss the implications and the limits of these assumptions in §4.

4 RESULTS: AGN/SB DECONVOLUTION AND REDSHIFT DEPENDENCE OF AGN ACTIVITY

The stacked spectra for the two samples of submm- and $24 \mu\text{m}$ -selected galaxies are shown in Fig. 1, together with

our deconvolution in the AGN and starburst components. The main results are the following.

- With only two free parameters, the deconvolution model reproduces the observed average spectral emission of high redshift sources in the 6-8 μm range, similarly to what happens for the low z ULIRGs analyzed in N08. We note that the simple fit we applied is strongly based on the assumption of little dispersion of the AGN and the starburst emission with respect to our templates. Therefore, it is not possible to extend the method to longer wavelengths (considering the redshift of our sources, we have a good spectral coverage up to $\sim 12 \mu\text{m}$) due to the presence of extra features (mainly the silicate absorption) which are well known to have quite different strengths from source to source.
- We quantitatively estimate the intrinsic AGN contributions in submm-ULIRGs to the 6 μm and bolometric luminosities: $\alpha_6 = 72.2^{+5.8}_{-7.1}\%$, $\alpha_{\text{bol}} = 6.9^{+2.3}_{-1.9}\%$, where the errors refer only to the formal statistical uncertainties in the fits.
- For the 24 μm -ULIRGs we find $\alpha_6 = 94.4^{+0.8}_{-1.0}\%$ and $\alpha_{\text{bol}} = 32.5^{+3.9}_{-3.6}\%$. It has already been suggested in previous studies (e.g., Sajina et al. 2007), and confirmed from the AGN and starburst 5–8 μm to bolometric ratios (N08), that 24 μm -ULIRGs are dominated by the AGN component. The new result presented here is that the starburst component is nevertheless present, and dominates the total bolometric luminosity.

The above results rely on a series of assumptions which need to be tested, in order to assess the reliability of our method. In particular, as mentioned in §3, our choice of the 5–8 μm rest-frame spectral interval is motivated by (1) the constancy of the AGN and starburst spectra, and (2) the high AGN/SB flux ratio in this band. These two properties are well measured for low-redshift sources, and the strongest assumption of our work is that they are both valid at higher redshifts and luminosities. Moreover, the possible intrinsic scatter in AGN and SB templates introduces additional uncertainties on top of the statistical errors in α_6 and α_{bol} . A further uncertainty has to be added to the estimate of α_{bol} due to the possible intrinsic scatter in the AGN and the SB bolometric ratios.

Following N08, it is possible to test the method and give a realistic estimate of the uncertainties by comparing the measured values of α_6 with the intrinsic 6 μm /bolometric ratio $R = L(6 \mu\text{m})/L_{\text{bol}}$. This new quantity has two interesting properties: 1) it depends only mildly from our spectral modeling (only through the AGN absorption τ_6) and never uses our assumptions on the bolometric ratios; 2) it is strongly sensitive to the AGN content, being (at low redshift) ~ 35 times higher in AGNs than in starbursts.

We plot R versus α_6 in Fig. 2. The most relevant results are: (1) the two quantities are correlated as expected, i.e. the sources with the highest α_6 also have the highest 6 μm /bolometric ratio; (2) the continuous line in Fig. 2 represents the best-fit correlation obtained by N08 for local ULIRGs, and the overall good match between the curve and our points suggests that there are no strong differences in bolometric ratios between low- and high- redshift sources. The dispersion of the single points from the relation is of the order of a factor ~ 2 , while the values for the composite spectra have a dispersion of ~ 10 -20%. We consider these as the best estimates of the errors involved in our analysis, and a confirmation of the validity of our approach.

Submm	α_6 [%]	α_{bol} [%]	24- μm	α_6 [%]	α_{bol} [%]
all	$72.2^{+5.8}_{-7.1}$	$6.9^{+2.3}_{-1.9}$	all	$94.4^{+0.8}_{-1.0}$	$32.5^{+3.9}_{-3.6}$
$z < 2.3$	0	0	$z < 2.3$	$93.3^{+1.3}_{-1.5}$	$28.6^{+4.9}_{-4.4}$
$z > 2.3$	$87.2^{+2.6}_{-3.2}$	$16.3^{+3.7}_{-3.2}$	$z > 2.3$	$95.6^{+1.0}_{-1.2}$	$38.5^{+6.8}_{-5.9}$
Reg.1	$88.5^{+2.8}_{-3.8}$	$18.1^{+5.1}_{-4.4}$	Reg.1	$95.5^{+1.1}_{-1.3}$	$37.8^{+6.8}_{-5.9}$
Reg.3	$45.4^{+15.2}_{-8.6}$	$2.3^{+1.9}_{-0.7}$	Reg.2	$92.8^{+1.7}_{-2.1}$	$26.9^{+6.0}_{-5.1}$
Reg.4	$83.5^{+5.0}_{-7.0}$	$12.7^{+5.4}_{-4.1}$	Reg.3	$94.1^{+1.9}_{-2.5}$	$31.6^{+9.2}_{-7.6}$

Table 2. Intrinsic AGN contribution to the 6 μm flux density, α_6 , and to the total infrared luminosity, α_{bol} in each group of submm and 24 μm sources discussed in the text. See Fig. 4 for the definition of Reg. 1-4.

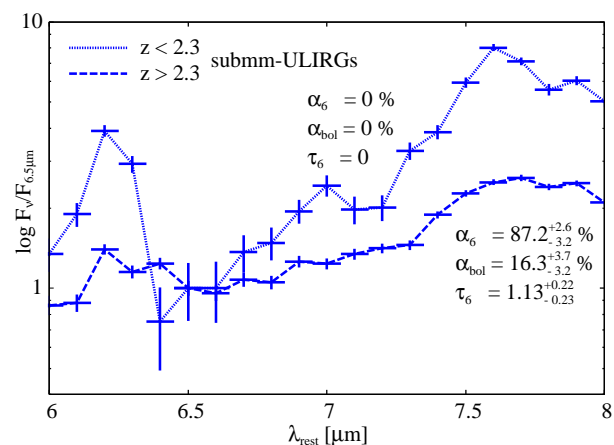


Figure 3. Same as the left panel of Fig. 1, for submm-ULIRGs at $z < 2.3$ (dotted lines) at $z > 2.3$ (dashed lines.) The flux density, F_ν are normalized at 6.5 μm .

In order to further investigate the issue of the AGN/SB content of high redshift galaxies, we analyzed the composite spectra obtained from different redshift and infrared luminosity intervals.

In Fig. 3, we show the composite spectra for the submm sources at $z < 2.3$ and $z > 2.3$, respectively ($z = 2.3$, is the submm-ULIRG median redshift of Chapman et al. (2005), and roughly divides our sample in two subsamples of similar size). It is apparent from Fig. 3 that the polycyclic aromatic hydrocarbon (PAH) emission features of lower- z ($z < 2.3$) submm-ULIRGs are stronger than those of higher- z ($z > 2.3$) galaxies. The AGN contribution is not needed in the fit of the low- z sample, while $(\alpha_6[\%], \alpha_{\text{bol}}[\%]) = (87.2^{+2.6}_{-3.2}, 16.3^{+3.7}_{-3.2})$ for the high- z sample.

This correlation needs to be checked for several selection/physical effects which could affect its significance and interpretation. In particular, we considered possible effects due to (1) selection, (2) K-correction, and (3) luminosity: 1) Selection effects. The submm galaxies in our sample are obtained from Chapman et al. (2005) and Valiante et al. (2007). The different selection criteria, based on radio pre-selection, lensing properties and submm flux are not expected to be relevant for our results. However, we note that almost all the Valiante et al. (2007) objects have $z > 2.3$ (Table 1), while those of Chapman et al. (2005) span the whole redshift range. In order to check whether the redshift effects in Fig. 3 are related to the properties of the two different

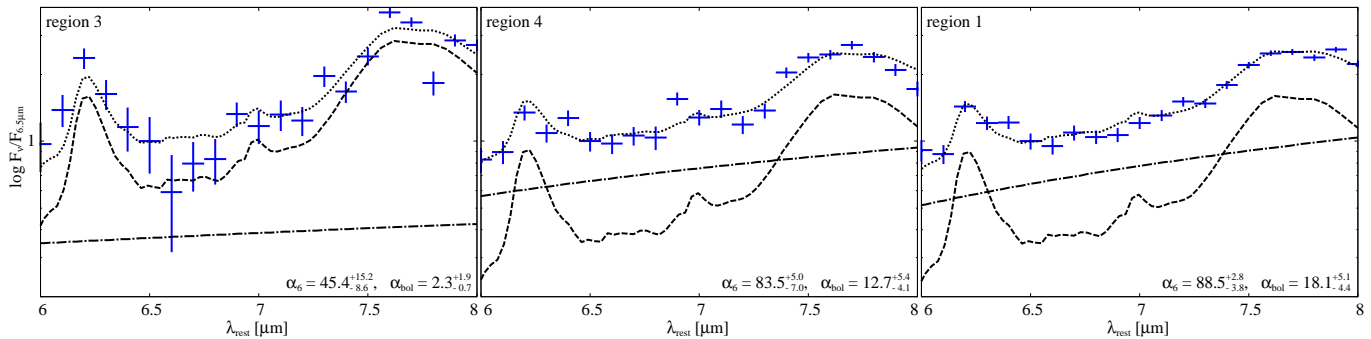


Figure 5. Same as the middle panel of Fig. 1, for different subgroups of submm-ULIRGs: low- z , low luminosity sources (*left*), high- z , low luminosity sources (*middle*), and high- z , high luminosity sources (*right*).

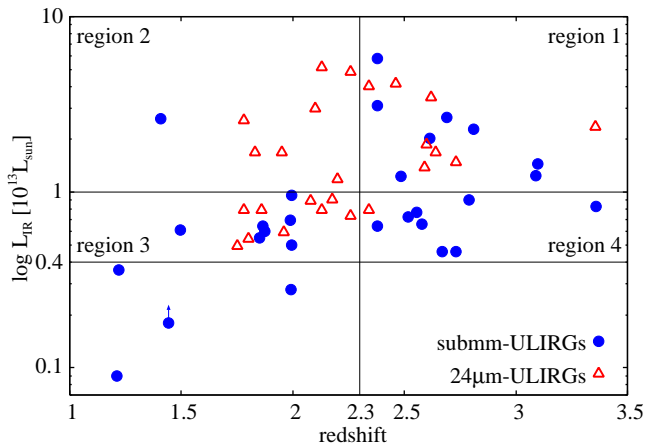


Figure 4. Luminosity–redshift plot for our samples of submm-ULIRGs (*blue filled circle*) and $24\ \mu\text{m}$ -ULIRGs (*red open triangle*). We define four regions delimited by the boundaries at $z = 2.3$, $L_{\text{IR}} = 0.4 \times 10^{13} L_{\odot}$ and $L_{\text{IR}} = 10^{13} L_{\odot}$.

samples, we repeated our analysis for the Chapman et al. (2005) sample only, obtaining results perfectly compatible with those in Fig. 3. In other words, no significant difference is found between the Valiante et al. (2007) and Chapman et al. (2005) objects at $z > 2.3$.

2) K-correction effects. The SCUBA $850\ \mu\text{m}$ selection does not seem to introduce any particular bias in favor of one of the two classes of sources: moving from redshift $z = 1.8$ to $z = 2.7$ (the median redshifts for the two subsamples of submm-ULIRGs), the observed central wavelength changes from $\lambda = 300\ \mu\text{m}$ to $\lambda = 230\ \mu\text{m}$. Indeed, we checked that there is no difference between the AGN and starburst bolometric ratios at these two wavelengths by using the SEDs of the ULIRGs classified as AGNs and starburst, respectively (Yang et al. 2007).

3) Luminosity effects. Since the AGN fraction in local ULIRGs increases with increasing infrared luminosity (Veilleux et al. 1997; Kim et al. 1998), our results may imply that the real physical trend is with luminosity, which is obviously partially degenerate with redshift. In order to check for this possibility, we analyze separately the luminosity and redshift dependence. In Fig. 4 we show the luminosity-redshift plot of our sample. Analyzing the population of the four highlighted regions, we note that we can

disentangle the luminosity and redshift effects by building composite spectra for submm-ULIRGs in regions 1 ($L > 10^{13} L_{\odot}$, $z > 2.3$), 3 ($L = 0.4 - 1 \times 10^{13} L_{\odot}$, $z < 2.3$) and 4 ($L = 0.4 - 1 \times 10^{13} L_{\odot}$, $z > 2.3$). The results of the fits of these templates are presented in Table 2. Objects in regions 1 and 4 are in the same redshift interval but have quite different luminosities, while sources in regions 3 and 4 have similar luminosities but different redshifts.

The spectra and the results are shown in Fig. 5. For submm-ULIRGs, the redshift dependence is confirmed by the comparison between the average spectra from the same luminosity range, while no strong luminosity dependence is found by comparing the composite spectra at $z > 2.3$. The increase of the AGN fraction with the redshift, and its constancy with the luminosity are also indicated by the average $6\ \mu\text{m}$ /bolometric ratios, plotted in Fig. 2 as a function of the average AGN contributions.

We have repeated the analysis the $L - z$ plane also for the $24\ \mu\text{m}$ sources, building composite spectra for Reg. 1, 2 and 3. The fit results presented in Table 2 indicate that no luminosity or redshift effect can be significantly detected.

5 CONCLUSIONS

We quantitatively estimated the relative AGN and starburst contributions in two samples of submillimeter- and $24\ \mu\text{m}$ -selected galaxies in the redshift range $z = 1 - 3$ by applying a deconvolution model based on AGN and starburst templates, already tested on low-redshift sources to the stacked $6 - 8\ \mu\text{m}$ spectra. We showed that the method gives consistent results on high redshift sources, suggesting that both the average $6 - 8\ \mu\text{m}$ spectra and the $6\ \mu\text{m}$ /bolometric ratios are similar in local and high redshift ULIRGs. Overall, we find that the starburst component is dominant in submm-ULIRGs both at $6\ \mu\text{m}$ and bolometrically. We find evidence of a higher AGN contribution in higher redshift ($z > 2.3$) submm-ULIRGs with respect to lower redshift ($1 < z < 2.3$) objects. The AGN component always dominates the mid-infrared emission in $24\ \mu\text{m}$ -ULIRGs, as already known from previous work. However, the starburst contribution to the total luminosity is of the same order, or slightly higher, than that of the AGN even in the $24\ \mu\text{m}$ -ULIRGs.

ACKNOWLEDGMENTS

We thank the anonymous reviewer for valuable comments. This work has been partly supported by grant prin-mur 2006025203.

REFERENCES

- Blain, A. W., Smail, I., Ivison, R. J., Kneib, J.-P., & Frayer, D. T. 2002, *Phys. Rep.*, 369, 111
- Brand, K., et al. 2007, *ApJ*, 663, 204
- Chapman, S. C., Blain, A. W., Smail, I., & Ivison, R. J. 2005, *ApJ*, 622, 772
- Dole, H., et al. 2001, *A&A*, 372, 364
- Draine, B. T. 1989, *Infrared Spectroscopy in Astronomy*, 290, 93
- Greve, T. R., et al. 2005, *MNRAS*, 359, 1165
- Holland, W. S., et al. 1999, *MNRAS*, 303, 659
- Houck, J. R., et al. 2004, *ApJS*, 154, 18
- Houck, J. R., et al. 2005, *ApJL*, 622, L105
- Jannuzi, B. T., & Dey, A. 1999, *Photometric Redshifts and the Detection of High Redshift Galaxies*, 191, 111
- Kim, D.-C., Veilleux, S., & Sanders, D. B. 1998, *ApJ*, 508, 627
- Lagache, G., Puget, J.-L., & Dole, H. 2005, *ARA&A*, 43, 727
- Le Floch, E., et al. 2005, *ApJ*, 632, 169
- Lonsdale, C. J., Farrah, D., & Smith, H. E. 2006, *Astrophysics Update* 2, 285
- Nardini, E., Risaliti, G., Salvati, M., Sani, E., Imanishi, M., Marconi, A., & Maiolino, R. 2008, *MNRAS*, 385, L130 (N08)
- Netzer, H., et al. 2007, *ApJ*, 666, 806
- Pope, A., et al. 2008, *ApJ*, 675, 1171
- Rieke, G. H., et al. 2004, *ApJS*, 154, 25
- Risaliti, G., et al. 2006, *MNRAS*, 365, 303
- Sajina, A., Yan, L., Armus, L., Choi, P., Fadda, D., Helou, G., & Spoon, H. 2007, *ApJ*, 664, 713
- Sanders, D. B., & Mirabel, I. F. 1996, *ARA&A*, 34, 749
- Smail, I., Ivison, R. J., & Blain, A. W. 1997, *ApJL*, 490, L5
- Soifer, B. T., et al. 1984, *ApJL*, 278, L71
- Swinbank, A. M., Smail, I., Chapman, S. C., Blain, A. W., Ivison, R. J., & Keel, W. C. 2004, *ApJ*, 617, 64
- Valiante, E., Lutz, D., Sturm, E., Genzel, R., Tacconi, L. J., Lehnert, M. D., & Baker, A. J. 2007, *ApJ*, 660, 1060
- Veilleux, S., Sanders, D. B., & Kim, D.-C. 1997, *ApJ*, 484, 92
- Yan, L., et al. 2005, *ApJ*, 628, 604
- Yang, M., Greve, T. R., Dowell, C. D., & Borys, C. 2007, *ApJ*, 660, 1198